Crystal and electronic structures and magnetic susceptibility of the photochemically prepared layered vanadyl phosphate Na(VO)$_2$(PO$_4$)$_2$·4H$_2$O †

Toshihiro Yamase* and Haruyo Makino

Research Laboratory of Resources Utilization, Tokyo Institute of Technology, 4259 Nagatsuta, Midori-ku, Yokohama 226-8503, Japan. E-mail: tyamase@res.titech.ac.jp

Prolonged photolysis of aqueous solutions containing Na$_3$VO$_4$, NaH$_2$PO$_4$, and MeOH at pH 1.8 adjusted by use of H$_3$PO$_4$ led to the formation of a layered vanadyl phosphate, Na(VO)$_2$(PO$_4$)$_2$·4H$_2$O **1**. A single-crystal X-ray structural analysis of a dark green crystal of **1** showed that the structure contains layers of vanadium (randomly with 1:1 ratio of V^{4+} and V^{5+}) and phosphorus oxide with the water molecules and sodium cations between the layers. The layer is a 4-connected net in which corner-sharing vanadium oxygen octahedra and phosphate tetrahedra alternate. The molecular structure is identical with that of a hydrothermally prepared Na$^+$ compound but reveals a non-zero dihedral angle (2.61°) between the least-squares planes (containing four equatorial oxygen atoms) of the VO$_6$ octahedra in contrast to the parallel arrangement of the basal least-squares planes for the latter. Magnetic susceptibility measurements for **1** show weak ferromagnetic coupling ($J/k = 0.87$ K) at $T \leq 100$ K and weak antiferromagnetic behavior at $T > 100$ K. The magneto/structural relationship for the retracted-chair-like V(OPO)$_2$V rings is compared among other layered vanadyl phosphate compounds. The ferromagnetic property of the d$_{xy}$ orbital at one V^{IV} in the retracted-chair V^{IV}(OPO)$_2$V^{IV} ring can be explained in terms of interaction with the V=O π* orbital at the opposite V^{IV}, which is possible when both distances of (O=)V$\cdots$V(=O) and (O=)V$\cdots$O(=V) are short ($\approx$4.55 and $\approx$4.36 Å, respectively). Otherwise, an antiferromagnetic property due to the superexchange interaction between magnetic d$_{xy}$ orbitals at both V^{IV} is operative. The results of extended Hückel (EH) calculations for a fragment model [V$_8$P$_8$O$_{40}$]$^{4-}$ (with V^{IV}/V^V = 1/1) support a variety of magnetic interactions of the unpaired electron at V^{IV} in the V–P–O layer consisting of the retracted-chair V(OPO)$_2$V rings.

Layered vanadyl phosphates, M$_x$VOPO$_4$·nH$_2$O (M = alkali or alkaline-earth metal), have bilayer structures intercalated by metal ions/water molecules. Each layer is composed of corner-sharing VO$_6$ octahedra and PO$_4$ tetrahedra.[4,5] Some of these intercalated materials are well known catalysts, and a few show unusual magnetic interactions.[6–9] For the majority of inter-calation compounds, complete structural determinations by single-crystal X-ray diffraction methods are unavailable; traditionally, powder X-ray diffraction is the principal method used to infer the orientation and steric relationships between the intercalant and the host lattice. Recently, however, hydrothermal reactions have been found to be an effective route to prepare intercalated materials as well as to grow suitable single crystals for structural characterization.[10–12] A systematic study on the magneto/structural relationship for the hydrothermally prepared vanadyl phosphates has concluded that a parallel arrangement of the basal least-square planes (containing four equatorial oxygen atoms) of the VO$_6$ octahedra is an important factor for ferromagnetic coupling:[7–9] the alkali-metal compounds Na(VO)$_2$(PO$_4$)$_2$·4H$_2$O, K(VO)$_2$(PO$_4$)$_2$·3H$_2$O, and Rb(VO)$_2$(PO$_4$)$_2$·3H$_2$O with a parallel arrangement of the VO$_6$ basal planes were ferromagnetic, while other vanadyl phosphate compounds such as VO(HPO$_4$)·2H$_2$O and Sr(VO)$_2$(PO$_4$)$_2$·4H$_2$O, with the VO$_6$ basal O$_4$ planes canted toward each other[11] were antiferromagnetic and showed that a smaller dihedral angle between the VO$_6$ basal O$_4$ planes was reflected in a smaller antiferromagnetic interaction. One can recall that the Na$^+$ compounds (Na$_{0.3}$VOPO$_4$·2H$_2$O, Na$_{0.5}$VOPO$_4$·2H$_2$O, and

NaVOPO$_4$·H$_2$O) which were prepared by the reaction of NaI with VOPO$_4$·2H$_2$O in acetone were antiferromagnetic.[13] Although the different magnetic interactions between two kinds of Na$_{0.5}$VOPO$_4$·2H$_2$O prepared by different methods implies that the magnetic behavior of M$_x$VOPO$_4$·nH$_2$O is preparation-sensitive due to subtle change in the structure, the mechanistic detail for such a difference in the magnetic interaction still remains unclear.[7] We have developed a photochemical encapsulation method, in which vanadate species such as [V$_4$O$_{12}$]$^{4-}$ and [VO$_4$]$^{3-}$ undergo photochemical self-assembly in the presence of charged or uncharged species as templates to yield spherical clusters encapsulating templates.[1–3] This method allows us to prepare a wide variety of structures for the poly-oxovanadates from spherical to layered ones. This paper describes the structure and ferromagnetic behavior of a layered vanadyl phosphate compound prepared by this method, Na(VO)$_2$(PO$_4$)$_2$·4H$_2$O **1**. The molecular structure of **1** is identical with that of the hydrothermally prepared Na$^+$ compound (**2**),[10] but reveals a non-zero dihedral angle (2.61°) between the VO$_6$ basal planes. This provides an appropriate opportunity to discuss the magnetic variability of vanadyl phosphate systems with relevance to their structures.

Experimental

Preparation and chemical analysis of compound 1

All the reagents were of at least analytical grade and used without further purification. The layered compound Na(VO)$_2$-(PO$_4$)$_2$·4H$_2$O **1** was prepared as follows: an aqueous solution containing Na$_3$VO$_4$ (0.25 g, 1.38 mmol) and NaH$_2$PO$_4$ (1.3 g, 10.8 mmol) in water (18 cm^3) in a Pyrex tube (20 cm^3) was adjusted to pH 1.8 with H$_3$PO$_4$ and MeOH (2 cm^3) was added.

DOI: 10.1039/a909452k

J. Chem. Soc., Dalton Trans., 2000, 1143–1150   **1143**

Table 1 Crystal and refinement data for $NaV_2P_2O_{10}\cdot 4H_2O$ **1**[a]

Formula	$H_8NaO_{14}P_2V_2$
M	418.88
Crystal symmetry	Triclinic
Space group	$P1$
a/Å	6.293(3)
b/Å	6.294(3)
c/Å	6.844(5)
α/°	107.04(5)
β/°	92.34(5)
γ/°	90.13(5)
U/Å^3	258.9(5)
Z	1
D_c/g cm^{-3}	2.686
μ/cm^{-1}	22.372
No. data measured	1633
R(int)	0.033
No. unique data	1508
No. observed data [$|F| > 3.0\ \sigma(F)$]	948
No. variables	89
R	0.056
R'	0.055

[a] The refinement in space group $P\bar{1}$ with anisotropic thermal parameters for all non-H atoms resulted in larger values of R ($R = 0.067$ and $R' = 0.072$), compared with the refinement in $P1$ with anisotropic thermal parameters for V and Na atoms. This may be due to the disorder of Na with a half occupancy in the case of $P\bar{1}$. In addition, the powder X-ray diffraction pattern of compound **1** did not show any peaks at lower angle ($2\theta < 13.5°$) corresponding to the doubling of the c axis. These results reveal that the choice of $P1$ and the cell parameters for **1** is reasonable and that the strongest peak ($d = 6.534$ Å) at $2\theta = 13.54°$ corresponds to (001) not (002). The CIF and Fig. 1S show the refinement data in $P\bar{1}$ and the powder X-ray diffraction patterns of **1** as Supporting Information.

The resulting solution was irradiated for 6 h under an atmosphere of nitrogen gas using a 500 W superhigh-pressure mercury lamp. Dark green orthorhombic single crystals were precipitated within 1 d with a yield of 25%. Crystalline **1** was also prepared by using $[NH_3Bu^t]_4[V_4O_{12}]$ instead of Na_3VO_4.

The vanadium content of compound **1** was determined by a potentiometric method. Measurements of the potential using a platinum indicator electrode *vs.* Ag–AgCl reference electrode at open circuit were carried out using a TOA Electronics IM-5S ion meter. The number of vanadium(IV) centers was unambiguously established by back titration analysis: a known excess of ammonium iron(II) sulfate was added to the sample in 1 mol dm^{-3} H_2SO_4 to reduce V^V to V^{IV} which was determined using a standard solution of $KMnO_4$. The potentiometric titrations of **1** gave one (1.0 ± 0.1)-electron reduction per $[(VO)_2(PO_4)_2]^-$ anion, which corresponds to the numbers of V^{IV} in the anion. Sodium was determined potentiometrically also on the TOA Electronics IM-5S ion meter combined with a NA-115B ion-selective electrode. Phosphorus analysis was carried out on a X-ray-fluorescence element analyzer (JEOL, JSX-3200). Thermogravimetric analysis using a Rigaku Thermoflex TG-DGC instrument was used for the determination of lattice water (Found: Na, 5.41; P, 15.2; V, 24.5. Calc. for $H_8NaO_{14}P_2V_2$: Na, 5.48; P, 14.8; V, 24.3%). The IR spectra were recorded on a JASCO FT/IR-5000 spectrometer, X-Band ESR on a JEOL RE1X ESR spectrometer equipped with an ES-CT470 continuous-helium-flow cryostat. The magnetic measurements were carried out on microcrystalline samples with a magnetometer (Quantum design, MPMS-5S) equipped with a SQUID sensor. The temperature range was 4–300 K, and the magnetic field was 1.0 T. The molar susceptibility was corrected for the diamagnetic contributions of **1** (-185×10^{-6} emu) using standard Pascal constants.[14]

X-Ray structural analysis

A crystal of compound **1** was mounted on a Rigaku AFC-5S diffractometer equipped with graphite crystal monochrom-

Table 2 Extended Hückel parameters used for the calculations

Atom	Orbital	H_{ii}/eV	ξ_1[a]
V	4s	−6.740	1.2480
	4p	−4.512	1.0410
	3d	−8.000	5.0519 (0.3738)
P	3s	−16.150	1.8160
	3p	−10.490	1.4780
	3d	−2.110	1.7310
O	2s	−28.480	2.1920
	2p	−13.620	2.0180

[a] Two Slater exponentials are listed for the V 3d functions. Each is followed in parentheses by the coefficient in the double-ζ expansion. $\xi_2 = 2.1728$ (0.7456).

atized Mo-Kα ($\lambda = 0.71069$ Å) radiation, and data were collected at 300 K. The structure was solved by direct methods and refined with full-matrix least squares on F (SHELXS 86).[15] Lorentz-polarization factors were applied and an absorption correction was made based on the isotropically refined structure, using the DIFABS program (correction factors of 0.82–1.08).[16] The V and Na atoms were refined with anisotropic thermal parameters. Anisotropic refinement for all non-H atoms was unsuccessful, probably because the crystal used for the intensity measurement was thin plate-shaped, approximately $0.2 \times 0.2 \times 0.02$ mm in size, which led to difficulty in the precise absorption correction. A summary of crystal data for **1** is shown in Table 1. All calculations were carried out on a Micro VAX II computer using the TEXSAN software package.[17]

CCDC reference number 186/1851.

See http://www.rsc.org/suppdata/dt/a9/a909452k/ for crystallographic files in .cif format.

The bond strength (s) in valence units was calculated using $s = (d/1.791)^{-5.1}$ and $(d/1.770)^{-5.2}$ for the V^V–O and V^{IV}–O bond length (d) in Å, respectively,[18] and the valence sum (bond order = Σs) of all of the V^V–O and V^{IV}–O bond strengths about a given O atom gives the valence of the atom. The alternative expression, $s = \exp[(d_0 - d)/B]$, where d_0 (= 1.803 and 1.784 Å for V^V and V^{IV} sites, respectively) and B (= 0.37) are empirically determined parameters,[19] gave similar bond-valence values.

Extended Hückel (EH) calculations

The EH calculations were performed using the CAChe program (Sony Tektronix). The atomic orbitals are simple Slater-type orbitals except for vanadium 3d orbitals where a linear combination of two Slater functions was chosen. The parameters for all atoms used are listed in Table 2. The Wolfberg–Helmholz proportionality constant was set at 1.75.

Results and discussion

Crystal structure

The structure of compound **1** contains layers of VO_6 octahedra/ PO_4 tetrahedra linkage anions and $[Na(H_2O)_4]^+$ cations between the layers, as shown in Fig. 1. The layer is a 4-connected net in which corner-sharing vanadium oxygen octahedra and phosphate tetrahedra alternate. Each vanadium octahedron shares its four equatorial oxygen atoms with four different PO_4 groups. The remaining axial oxygen consists of a vanadyl oxygen and a water molecule co-ordinated *trans* to it. Along the [110] direction the vanadyl oxygens alternatively point up and down relative to a layer, to make a linkage of the "retracted chair"-like $V(OPO)_2V$ rings which are folded with the orientation of the vanadyl oxygens retracted into the ring structure, as shown in Fig. 2.[20] The interlayer separation for Na$^+$ and water is 6.53 Å, which is the same as for **2**.[10] Table 3 shows selected bond distances and angles, and dihedral angles between the VO_6 basal O_4 and $Na(H_2O)_4$ least-squares planes. The V atoms have
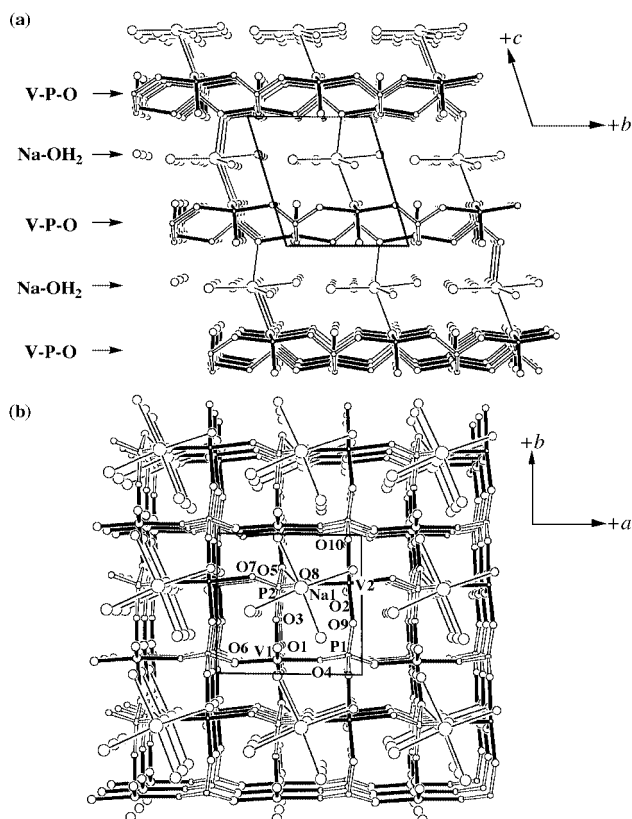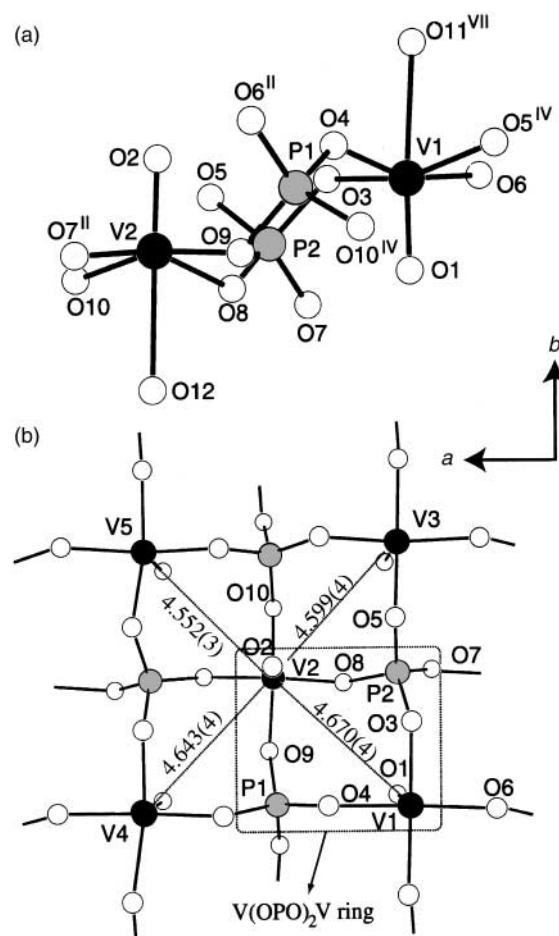
Fig. 1 Structure of compound **1** as viewed (a) along the *a* axis and (b) along the *c* axis. Vanadium is octahedrally co-ordinated, and phosphorus is tetrahedrally co-ordinated. The V–O bonds are drawn as thick lines and P–O bonds as double lines.

Fig. 2 Retracted chair conformation of $[(VO)_2(PO_4)_2]^-$ (a) and a section of a 4-connected net (b) in compound **1**. Water O atoms O11 and O12 and Na(H$_2$O)$_4$ are omitted for clarity in (b), where V···V distances (in Å) are indicated. Symmetry keys: II (*x* + 1, *y*, *z*), IV (*x*, *y* − 1, *z*), and VII (*x*, *y* − 1, *z* − 1).

a common environment of a grossly distorted octahedron; one short V–O bond length is 1.54(2)–1.59(2) Å, which is about 0.39 Å shorter than the four equatorial V–O bonds (1.91(2)–2.01(2) Å, average 1.96 Å), but the sixth bond with water oxygen atom is much longer, 2.38(2)–2.40(2) Å. Bond order sums of V–O bonds are in good accord with their average formal oxidation states (4.5). The vanadium-(v) and -(iv) ions are probably disordered inside the layers. The dihedral angle between the basal least-squares planes containing four equatorial oxygen atoms of the VO$_6$ octahedra in the V(OPO)$_2$V ring is 2.61°, in contrast to the case of **2** (with a parallel configuration of the VO$_6$ basal planes).[10] Each Na$^+$ ion is octahedrally co-ordinated in a highly distorted fashion, with four water oxygens and two phosphate oxygens (Fig. 1(a)). The least-squares plane of the Na(H$_2$O)$_4$ moieties is almost parallel to the VO$_6$ basal O$_4$ least-squares planes in the layer, making an average angle of 0.8° (0.3–1.4°). This angle is significantly smaller than for **2** (average 6.3°, 6.2–6.4°).[10] In both **1** and **2** the V–P–O layers do not stack directly on top of each other so that each V=O group is not oriented toward the water molecule co-ordinated *trans* to the V=O group of an adjacent layer, but adjacent layers are offset. It should be noted that the structure of **1** has a different layer stacking sequence from that found in **2**: in the former all atoms of the same kind (*e.g.*, all V or all P) form strings parallel with the triclinic *c* axis (Fig. 1), while in the latter alternating V and P atoms lie in strings parallel with the triclinic *c* axis. This results in doubling of the *c* axis in the latter relative to that in the former.[10]

Magnetic susceptibility

Fig. 3(a) and (b) show the variation of reciprocal molar magnetic susceptibility (χ^{-1}) *vs.* temperature for compound **1** at 100 < *T* < 350 and 4.2 < *T* < 100 K, respectively. The data approximately obey the Curie–Weiss law $\chi = C/(T - \theta)$. The slope of the line is the Curie constant (*C*), and the intercept is

the Weiss constant (θ). Although an approximately linear fitting of χ^{-1} against *T* at 4.2 < *T* < 350 K gives a positive value of θ (= +0.4 K) with *C* = 0.344 and suggests a ferromagnetic interaction which is consistent with the behavior observed for **2**,[7] the magnetic susceptibility at *T* > 100 K shows an antiferromagnetic interaction on the basis of a negative Weiss constant of θ = −8.0 K with *C* = 0.356 (Fig. 3(a)). On the other hand, the magnetic susceptibility at *T* < 100 K shows a ferromagnetic interaction with θ = +1.8 K and *C* = 0.335 (Fig. 3(b)). The observation of antiferromagnetic behavior at *T* > 100 K has been reported for Na$^+$ compounds prepared by reaction between NaI and VOPO$_4$·2H$_2$O.[13] Fig. 4(a) shows a plot of the χT product against *T* below 100 K, indicating a strong increase below 50 K, and confirms the ferromagnetic nature. Fig. 4(b) shows the 4.2 K ESR spectrum which exhibits $g_\perp \approx 1.990$ and $g_\parallel \approx 1.889$. A simple two-dimensional Heisenberg model for ferromagnetic square planar lattices of M$_x$VOPO$_4$·nH$_2$O[21,22] gives a reasonable fit to the data (Fig. 4(a)) with *J/k* = 0.87(1) K and *g* = 1.898(1). The calculated value *J/k* = 0.87(1) K is in good agreement with the observed θ = +1.8 K which represents theoretically twice the *J/k* value in a two-dimensional Heisenberg model. In this calculation the couplings between the V–P–O planes were not taken into consideration. The Curie constant observed at *T* < 100 K is about 7% lower than that (= 0.359) expected from the average *g* value ($\langle g \rangle \approx 1.956$ at 4.2 K) obtained by the ESR spectrum. The effective magnetic moment calculated from the Curie constant, 1.64 μ_B, is close to the value (1.73 μ_B) expected for an isolated V^{4+} ion (3d^1, *S* = 1/2). The 4.2 K ESR spectrum of **1** showed neither hyperfine pattern nor zero-field splitting associated with exchange only in the isolated pair of vanadyl centers within the cluster. The broad ESR

Table 3 Selected bond distances (Å) and angles (°), and dihedral angles (°) between least-squares planes (O7, O8, O9, O10) or (O3, O4, O5, O6) and (Na1, O11, O12, O13, O14)

V(1)–O(1)	1.59(2)	P(1)–O(4)	1.55(2)	Na(1)–O(4)	2.61(2)
V(1)–O(3)	1.98(2)	P(1)–O(6^{II})	1.52(2)	Na(1)–O(10^{VII})	2.58(2)
V(1)–O(4)	1.91(2)	P(1)–O(9)	1.58(2)	Na(1)–O(11)	2.49(2)
V(1)–O(5^{IV})	1.98(2)	P(1)–O(10^{IV})	1.57(2)	Na(1)–O(12)	2.51(2)
V(1)–O(6)	1.92(2)	P(2)–O(3)	1.47(2)	Na(1)–O(13)	2.48(1)
V(1)–O(11^{VII})	2.38(2)	P(2)–O(5)	1.50(2)	Na(1)–O(14)	2.40(2)
V(2)–O(2)	1.54(2)	P(2)–O(7)	1.54(2)		
V(2)–O(7^{II})	2.01(2)	P(2)–O(8)	1.53(2)		
V(2)–O(8)	1.98(1)				
V(2)–O(9)	1.95(2)				
V(2)–O(10)	1.93(2)				
V(2)–O(12)	2.40(2)				
O(1)–V(1)–O(3)	99.2(8)	O(3)–V(1)–O(4)	88.0(8)	O(3)–V(1)–O(11^{VII})	77.7(7)
O(1)–V(1)–O(4)	98.1(8)	O(3)–V(1)–O(5^{IV})	163.9(9)	O(4)–V(1)–O(11^{VII})	81.1(7)
O(1)–V(1)–O(5^{IV})	96.8(8)	O(4)–V(1)–O(5^{IV})	88.1(8)	O(5^{IV})–V(1)–O(11^{VII})	81.8(4)
O(1)–V(1)–O(6)	100.7(8)	O(5^{IV})–V(1)–O(6)	89.4(7)	O(6)–V(1)–O(11^{VII})	80.0(7)
O(2)–V(2)–O(9)	97.9(9)	O(8)–V(2)–O(7)	159.6(7)		
O(2)–V(2)–O(8)	102.3(9)	O(2)–V(2)–O(12)	178.0(9)		
O(2)–V(2)–O(10)	100(1)	O(8)–V(2)–O(7^{II})	159.6(7)		
O(2)–V(2)–O(7^{II})	98(1)	O(9)–V(2)–O(10)	162.4(9)		
O(11)–Na(1)–O(12)	93.8(6)	O(4^V)–Na(1)–O(11)	66.8(6)	O(10^{VII})–Na(1)–O(11)	117.5(7)
O(11)–Na(1)–O(14)	91.3(5)	O(4^V)–Na(1)–O(12)	79.3(6)	O(10^{VII})–Na(1)–O(12)	68.7(6)
O(12)–Na(1)–O(13)	90.0(6)	O(4^V)–Na(1)–O(13)	105.8(6)	O(10^{VII})–Na(1)–O(13)	71.7(6)
O(13)–Na(1)–O(14)	85.5(5)	O(4^V)–Na(1)–O(14)	105.6(5)	O(10^{VII})–Na(1)–O(14)	106.1(5)
O(13)–Na(1)–O(11)	170.8(6)	O(4^V)–Na(1)–O(8)	59.8(3)	O(14)–Na(1)–O(12)	174.0(5)
V(1)···V(2)	4.670(4)	V(1)···V(2^{III})	4.643(4)	V(1)···V(2^{IV})	4.599(4)
V(1)···V(2^{VI})	4.552(3)	V(1)···O(2^{VI})	4.36(2)	V(1)···O(2^{IV})	4.50(2)
V(1)···O(2^{III})	4.43(2)	V(1)···O(2)	4.56(2)	V(1)···O(1^{VIII})	4.36(2)
V(1)···O(1^{II})	4.56(2)	V(1)···O(1^V)	4.38(2)	V(1)···O(1)	4.56(2)
(Na1, O11, O12, O13, O14)	/	(O7^{II}, O8, O9, O10)	5.34		
	/	(O3, O4, O5^{IV}, O6)	4.39		
(O7^{II}, O8, O9, O10)	/	(O3, O4, O5^{IV}, O6)	2.61		

Symmetry codes: II $x + 1, y, z$; III $x − 1, y, z$; IV $x, y − 1, z$; V $x, y + 1, z$; VI $x − 1, y − 1, z$; VII $x, y − 1, z − 1$; VIII $x + 1, y + 1, z$.
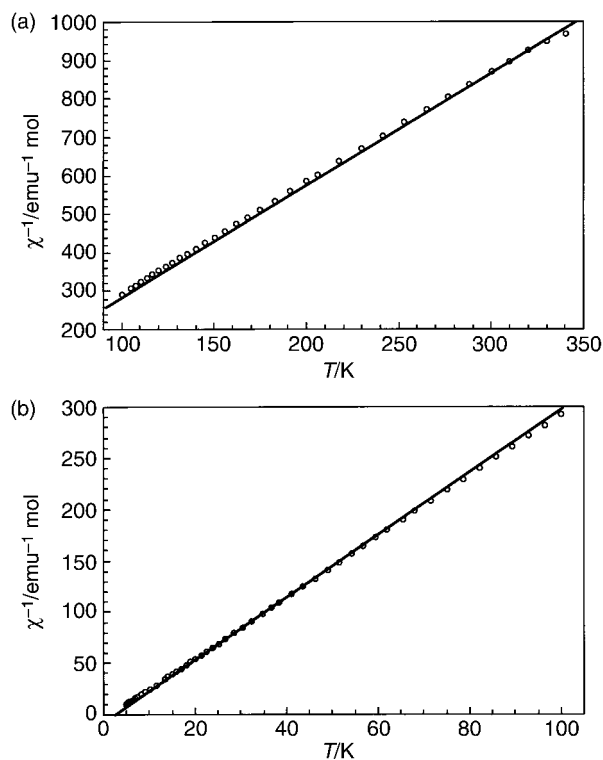

Fig. 3 Reciprocal susceptibilities *vs.* temperature variations in the ranges 100–350 (a) and 4–100 K (b).

signal indicative of very weak extended exchange interactions of the paramagnetic electrons over the V–P–O plane is due to the fact that the hopping frequency of the paramagnetic electrons becomes larger than the hyperfine coupling constant $((2–3) × 10^2$ MHz$)^1$ expressed in frequency units. A similar spectrum can be also produced in ferromagnetic α-VOSO₄ solids.[22]

Structural comparison with other layered vanadyl phosphates

The magneto/structural relationship among the hydrothermally prepared vanadyl phosphate compounds has revealed that the VO₆ basal O₄ planes in the V–P–O layers for the ferromagnetic compounds are arranged to be parallel.[7–9] In **1**, characterized as a ferromagnetic compound (Fig. 4), however, the dihedral angle between the least-squares VO₆ basal O₄ planes of the V(OPO)₂V rings is 2.61° which is rather large compared to that for a typical antiferromagnetic compound, Sr(VO)₂(PO₄)₂· 4H₂O (2.39°).[7,11] The complexity of the problem seems to result from the fact that the ferro- and antiferro-magnetic exchange interactions are small enough to be affected by a slight variation of the structure. The V–P–O layer network for **1** constitutes four distinct nearest neighbor V(OPO)₂V rings with the retracted chair arrangement (Fig. 2(b)). The V···V distances in the V(OPO)₂V rings with the retracted chair geometry are 4.552(3), 4.599(4), 4.643(4), and 4.670(4) Å, which are in response to a variation of the dihedral angle (129.1, 130.5, 134.2, and 135.3°, respectively) between the VO₆ basal O₄ plane and the bridging O₄ planes for the four neighboring V(OPO)₂V rings. In the retracted-chaired conformation of the V(OPO)₂V ring the vanadyl oxygen of one metal center lies close to, but slightly below, the V-containing least-squares equatorial plane of the opposite center (Fig. 2(a)). With this geometry, the unpaired electron in the d_{xy} orbital of one V^{IV} can delocalize by direct overlap into the V=O π* system of the other, which is reflected in the (O=)V···O(=V) distance between the two metal centers. Since the V=O π* orbital is orthogonal to its own mag-
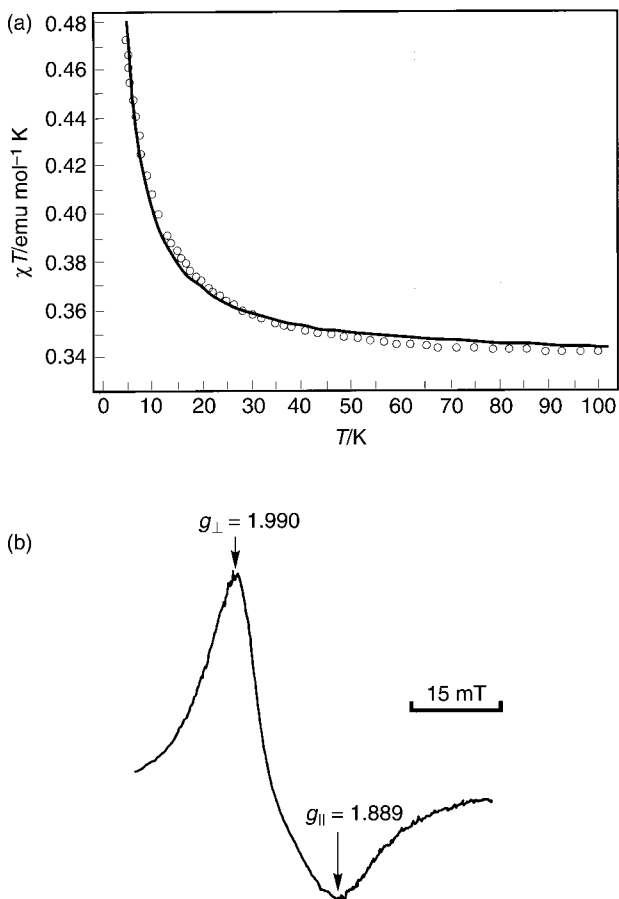
Fig. 4 (a) Plot of χT *vs.* T for compound **1** below 100 K. (b) The ESR spectrum of **1** at 4.2 K.
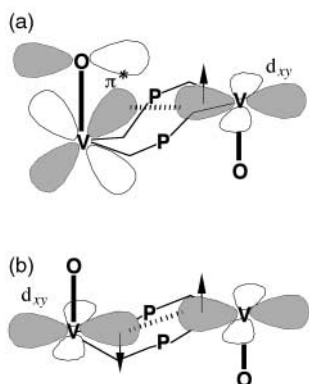
Fig. 5 Ferro- (a) and antiferro- (b) magnetic interaction of the unpaired electron at V^{IV} in the retracted $V^{IV}(OPO)_2V^{IV}$ ring.

netic orbital (if $V^{IV}=O$), the resulting exchange coupling would be ferromagnetic to satisfy Fund's rule. As the retracted-chair geometry is bent back toward longer $V \cdots V$ distances, the $d_{xy} \cdots V=O$ π^* overlap will decrease while the $d_{xy} \cdots d_{xy}$ overlap will increase. Overlap of the two vanadyl magnetic orbitals results in antiferromagnetic coupling which would be due to the superexchange interaction between the two V^{IV}.[20] Fig. 5 shows schematic representations for the ferro- (a) and antiferro- (b) magnetic effects due to the proposed orbital interaction of the unpaired electron at V^{IV} in the retracted $V(OPO)_2V$ rings. Structural details of the V–P–O layer were compared among five layered vanadyl phosphate compounds with similar retracted $V(OPO)_2V$ rings: **1**, **2**,[10] Rb(VO)$_2$(PO$_4$)$_2$·3H$_2$O **3**,[7] Sr(VO)$_2$(PO$_4$)$_2$·4H$_2$O **4**,[11] and VO(HPO$_4$)·4H$_2$O **5**.[23] Table 4 lists the $V \cdots V$ distances in the four neighboring $V(OPO)_2V$ rings, the $(O=)V \cdots O(=V)$ distances of the vanadyl V atom from the opposite vanadyl O atom in the corresponding $V(OPO)_2V$ ring, the dihedral angles between the VO_6 basal O_4

planes in the $V(OPO)_2V$ ring, and the average gap between the neighboring layers for **1–5**. The structural variation by the insertion of M(H$_2$O)$_4$ (M = Na or Sr) or M(H$_2$O)$_3$ (M = Rb) moieties between the layers indicates that the magnitude of the average gap is affected by both size and charge (due to the electrostatic interaction) of intercalating metal cations. In **5** there was no interlayered co-ordination structure: each vanadyl octahedron shares an oxygen atom with the phosphate tetra-hedron in a parallel single chain, thus forming the infinite covalently linked double chain which is connected by the hydrogen bonding network.[23] The magnetic properties for **1–5** can be correlated with the structural fact that short distances of both $(O=)V \cdots V(=O)$ and $(O=)V \cdots O(=V)$ in the $V(OPO)_2V$ ring are required for the ferromagnetic coupling between d_{xy} orbitals in the $V^{IV}(OPO)_2V^{IV}$ ring: the ferromagnetic coupling in **1–3** occurs at the $V(OPO)_2V$ rings with the $V \cdots V$ (4.54–4.55 Å) and $V \cdots O$ (4.34–4.36 Å) distances, while in **4** and **5** consisting of the $V(OPO)_2V$ rings with slightly longer $V \cdots V$ distances (>4.58 Å) with an accompanying enlongation of the $V \cdots O$ distances (>4.38 Å) the antiferromagnetic interaction between the d_{xy} orbitals occurs.‡ As shown in Fig. 3(a), the antiferromagnetic property assigned on the basis of a small negative Weiss constant over a range of relatively high temper-atures (T = 100–350 K) may be ascribed to the $V^{IV} \cdots V^{IV}$ superexchange interaction at the $V(OPO)_2V$ rings with the $V \cdots V$ distances of >4.58 Å and the $V \cdots O$ distances of >4.38 Å for **1**. In fact, the χT plot against T in the range $4.2 < T < 350$ K for **1** indicated a crossover point from antiferro- to ferro-magnetic coupling around 120 K where a magnetic phase transition was suggested. Thus, the above scenario (Fig. 5) about the magneto/structural relationship for the retracted-chair conformation of the $V(OPO)_2V$ ring seems to work successfully (Table 4).

Electronic structure

To gain some insight into the electronic states of compound **1**, extended Hückel (EH) calculations were carried out for a fragment model $[V_8P_8O_{40}]^{4-}$ (with $V^{IV}/V^V = 1/1$), as shown in Fig. 6, where to simplify the calculation the contribution of Na$^+$ cations and water molecules in the interlayer was neg-lected. Cartesian coordinates were used. The crystallographic a axis was chosen as the Cartesian X axis, and Y axis lay along $b \sin \gamma$ on the plane perpendicular to the a axis. From these calculations, the first large gap occurs at -12.972 eV and separ-ates the V–O bonding levels from the mainly d orbitals between -7.872 and -5.880 eV, what we call the d band (consisting of forty MO levels with small energy gaps between each other within a band width of 1.992 eV). In this d band the XY sub-band, which corresponds to the HOMO for the unpaired elec-tron on the V and consists of a bunch of mainly V d_{xy} orbitals, is positioned in the range -7.872 to -7.706 eV. Subsequently, the YZ and ZX subbands consisting of mainly V d_{yz} and d_{zx} orbitals respectively in the range -7.617 to -7.246 eV, and the Z^2 and $X^2 - Y^2$ bands consisting of mainly V d_{z^2} and $d_{x^2-y^2}$ orbitals respectively in the range -7.102 to -5.880 eV. In Fig. 7(a) are presented the electronic energy levels for the V–P–O network fragment, several gaps being observed. Fig. 7(b) shows a diffuse reflectance spectrum of **1**, with peaks around 740 and 1400 nm. At low energy more negative than -12.972 eV, a bunch of levels comprising V–O bonding orbitals and O 2p dangling lone-pair orbitals are filled. The highest MO among these, MO_{160} at -12.972 eV, consists of a linear combination of p-type lone-pair orbitals for the bridging O atoms. The V=O bonding orbital containing $d\pi$–$p\pi$ bonding can be exemplified

Table 4 Structural comparison in $V \cdots V$ and $(O{=})V \cdots O({=}V)$ distances (Å) for the vanadyl atoms of the $V(OPO)_2V$ rings, dihedral angles (°) between the VO_6 basal O_4 planes, and the average gap (Å) between neighboring V–P–O layers among compounds **1–5**

	Ferromagnetic Na(VO)$_2$(PO$_4$)$_2$·4H$_2$O **1**	Ferromagnetic Na(VO)$_2$(PO$_4$)$_2$·4H$_2$O **2**	Ferromagnetic Rb(VO)$_2$(PO$_4$)$_2$·3H$_2$O	Antiferromagnetic Sr(VO)$_2$(PO$_4$)$_2$·4H$_2$O **4**	Antiferromagnetic VO(HPO$_4$)·4H$_2$O **5** [23]
$V \cdots V$	4.552(3)^a 4.599(4) 4.643(4) 4.670(4)	4.5473(9)^b 4.596(9) 4.627(9) 4.6646(9)	4.543(2) 4.557(2) 4.670(2) 4.705(2)	4.605(3) 4.627(4) 4.674(4) 4.680(3)	4.579(3) 4.595(3)
$V \cdots O$	4.36(2) 4.36(2)^c 4.50(2) 4.54(2) 4.43(2) 4.56(2) 4.56(2) 4.56(2)	4.379(2) 4.445(2) 4.478(2) 4.534(2)	4.356(5) 4.371(5) 4.541(5) 4.577(5)	4.387(9) 4.550(9)^c 4.385(1) 4.55(1) 4.52(1) 4.69(1) 4.514(9) 4.668(9)	4.380(6) 4.535(6) 4.445(9) 4.520(9)
Dihedral angle (°)	2.61	0	0	2.39	6.66
Gap (Å) between the V–P–O layers	4.67	4.67	4.98	4.50	—

^{a} Distances are V(2)···V(5), V(2)···V(4), V(2)···V(3), and V(2)···V(1) in Fig. 2(b) where V(5), V(4), and V(3) indicate V(1) atoms related by symmetry codes $(x - 1, y - 1, z)$, $(x - 1, y, z)$, and $(x, y - 1, z)$, respectively, that correspond to Fig. 6. ^{b} Distances for two crystallographically different V–P–O layers. ^{c} A set of two different distances is listed for each V(OPO)$_2$V ring.
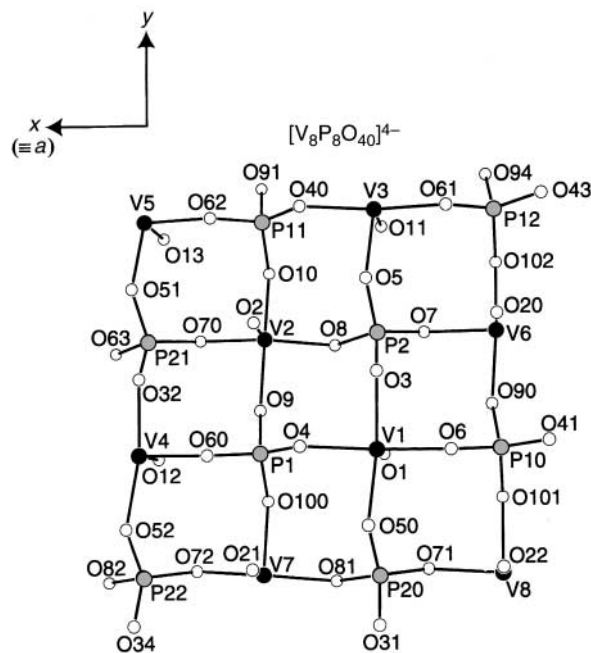
Fig. 6 The fragment $[V_8P_8O_{40}]^{4-}$ (with $V^{IV}/V^V = 1/1$) and reference axes used for the EH calculation. The contribution of Na$^+$ cations and water molecules in the interlayer was neglected.
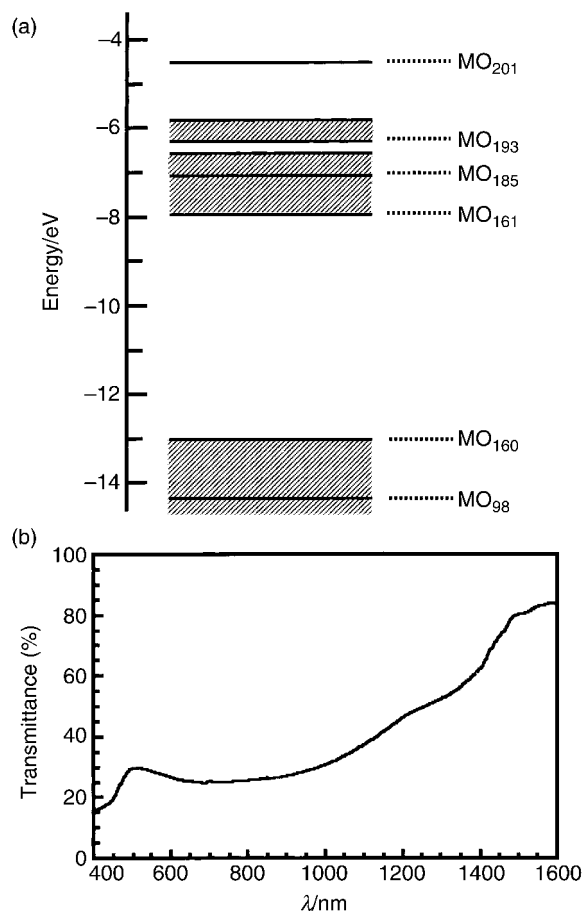

Fig. 7 Electronic energy-level scheme (a) for the fragment $[V_8P_8O_{40}]^{4-}$ (with $V^{IV}/V^V = 1/1$) and diffuse reflectance spectrum (b) of compound **1**.

by MO$_{111}$ at -13.598 eV, and two antibonding orbitals containing V=O π^* bonding, MO$_{183}$ at -7.246 eV, and V=O σ^* bonding, MO$_{193}$ at -6.256 eV. Orbital combination patterns of $[V_8P_8O_{40}]^{4-}$ (with $V^{IV}/V^V = 1/1$) for selected molecular orbitals are shown in Fig. 8 where main contributions from atomic orbitals of V and O for MO$_{98}$, MO$_{161}$, and MO$_{175}$ are combined with each other. Four magnetic HOMO electrons out of 324

Table 5 Computed energy levels (eV) and predominant atomic orbital coefficients of the selected MO for the fragment model $[V_8P_8O_{40}]^{4-}$ (Fig. 6)[a]

		MO_{98}	MO_{111}	MO_{160}	MO_{162}	MO_{166}	MO_{167}	MO_{183}	MO_{193}
Energy level (eV)		−13.723	−13.598	−12.972	−7.848	−7.769	−7.725	−7.246	−6.256
V(1)	d_{xy}						−0.609		
	d_{yz}		0.044						
V(2)	d_{xy}					0.116	−0.769		
	d_{zx}							−0.703	
	$d_{x^2-y^2}$						0.110		
V(3)	d_{xy}					−0.211			
	d_{yz}		−0.038						
	d_{z^2}		0.042						
V(4)	p_z								−0.326
	d_{xy}					0.926			
	$d_{x^2-y^2}$								0.381
	d_{z^2}								0.864
V(5)	d_{xy}				−0.974				
	d_{yz}	−0.048							
	$d_{x^2-y^2}$				0.140				
V(6)	d_{xy}					0.102			
	d_{zx}		−0.037						
	d_{z^2}		0.049						
V(7)	d_{xy}					−0.221			
	d_{zx}							−0.702	
	d_{z^2}								−0.100
V(8)	d_{zx}	0.057							
O(1)	p_x	−0.110							
	p_y		0.345						
	p_z	−0.117	−0.154						
O(2)	p_x	−0.216	−0.289					−0.199	
O(3)	p_y			−0.296					
	p_z		−0.112						
O(4)	p_y			−0.214					
O(5)	p_y		−0.166	−0.282					
	p_z		−0.186						
O(6)	p_y	−0.157		−0.129					
O(7)	p_x		0.159						
	p_y			−0.164					
	p_z		0.213						
O(8)	p_x			0.109					
	p_y			−0.209					
	p_z		0.142						
O(9)	p_x			0.109					
	p_y			−0.281					
O(10)	p_y			−0.208					
O(11)	p_x	0.104							
	p_y	0.205	−0.316						
	p_z		−0.144						
O(12)	p_x	0.115							
	p_y	−0.169	−0.191						
	p_z								0.298
O(13)	p_x	0.126							
	p_y	−0.364	0.141						
	p_z	0.102							
O(20)	p_x	−0.108	0.275						
	p_y								
	p_z		0.175						
O(21)	p_x	−0.241	0.129					−0.199	
	p_y	0.123							
O(22)	p_x	−0.417	−0.117						
	p_y	−0.164							
	p_z	0.162							
O(31)	p_x	−0.183							
	p_y		−0.111	−0.189					
O(32)	p_y			−0.101					−0.145
O(40)	p_y			−0.136					
O(41)	p_x	0.133							
O(50)	p_y			−0.205					
O(52)	p_y			−0.107					0.138
O(60)	p_y			−0.197					
O(61)	p_x			0.106					
	p_y			−0.109					
	p_z			−0.110					
O(62)	p_y				−0.102				
O(63)	p_y	−0.103							
	p_z		−0.106						
O(70)	p_y			−0.102					
O(71)	p_y	−0.112							
O(81)	p_y	0.112							
O(90)	p_x	−0.188							
	p_y			−0.121					
O(91)	p_y			−0.211					
O(94)	p_y			−0.165					
O(100)	p_y			−0.230					
O(101)	p_x	0.101							
	p_y			−0.105					
O(102)	p_x			0.105					
	p_y			−0.147					

[a] Atomic orbitals with their orbital coefficients of more than 0.1 (less than −0.1) are indicated. For $MO_{98,111,160}$, vanadium d orbitals with their orbital coefficients of more than 0.04 (less than −0.04) are also indicated.
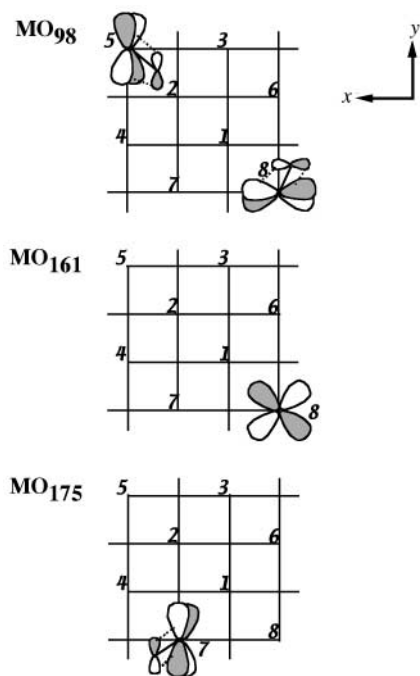
Fig. 8 Orbital combination patterns of the fragment $[V_8P_8O_{40}]^{4-}$ (with $V^{IV}/V^V = 1/1$) net for selected molecular orbitals: MO_{98} (a), MO_{161} (b), and MO_{175} (c). Numbers in the net indicate the V atoms denoted in Fig. 6.

valence electrons are considered to occupy the almost eightfold degenerate XY subband (MO_{161}–MO_{168}) and to be positioned separately at each MO. Table 5 shows the computed energy levels (in eV) and predominant atomic orbital coefficients for the selected molecular orbitals, MO_{98}, MO_{111}, MO_{160}, MO_{162}, MO_{166}, MO_{167}, MO_{183}, and MO_{193}. In the YZ/ZX or $Z^2/(X^2 - Y^2)$ subband the vanadyl O p orbitals are antibonding with the V $d_{yz/zx}$ or $d_{z^2/x^2 - y^2}$ orbitals, and the extent of the antibonding between the vanadyl atoms is much stronger than in the XY subband where none of the V d_{xy} orbitals is mixed with the vanadyl O p orbitals (Fig. 8 and Table 5). The orbital mixing expected among the subbands undoubtedly leads to a large transition probability (at the range of transition energy 0.60–1.99 eV) between the XY and $Z^2/(X^2 - Y^2)$ subbands due to the parity-allowed electric-dipole transition, as supported by the observation of the electronic transition with large intensities at *ca.* $\lambda_{max} = 740$ nm (= 1.68 eV) and *ca.* $\lambda_{sh} = 1400$ nm (= 0.89 eV) (Fig. 7(b)). The presence of several other transitions with similar energies seems to demonstrate a broadening of the absorption bands. The small difference in transition energy between the XY and YZ/ZX subbands suggests a favorable interaction of the d_{xy} orbital with V=O π^* orbitals. The ferromagnetic d_{xy} orbital at one V^{IV} of the retracted-chair $V^{IV}(OPO)_2V^{IV}$ ring with the shortest $V\cdots V$ and $V\cdots O$ distances (4.552(3) and 4.36(2) Å, respectively) appears at MO_{162} where the d_{xy} orbital at the V(5) center contributes with 0.97 wavefunction coefficient (Table 4). This MO_{162} could interact with the YZ/ZX subband orbitals (MO_{181}, MO_{182}, MO_{183}, and MO_{184}) which comprise the V=O π^* bonding at the opposite V(2) center in the $V(5)^{IV}(OPO)_2V(2)^{IV}$ ring, resulting in ferromagnetic interaction with the d_{xy} orbital at V(2) (corresponding to MO_{167}). Table 3S shows the computed energy levels (in eV) and predominant atomic orbital coefficients for MO_{163}, MO_{164}, MO_{168}, MO_{181}, MO_{182}, and MO_{184} as Supporting Information. The antiferromagnetic coupling arises from a direct $d_{xy}\cdots d_{xy}$ superexchange interaction. Such an interaction would be possible between MO_{163} (or MO_{164}) [containing a predominant distribution of the d_{xy} orbital at the V(6) (or V(7)) center] and MO_{168} (with a dominant combination between V(1) and V(2) d_{xy} orbitals) at the $V(1)^{IV}(OPO)_2V(6)^{IV}$ (or $V(1)^{IV}(OPO)_2V(7)^{IV}$) ring with the long $V\cdots V$ distance 4.643(4) (or 4.599(4)) Å, that

would occur at temperatures >100 K. Therefore, the ferromagnetic coupling in the V–P–O network for **1** occurs along the [110] direction, while the antiferromagnetic superexchange interaction occurs along the [1$\bar{1}$0] direction. The contribution of the d_{xy} orbitals of P(2) and P(10) centers to MO_{163} and MO_{168} was small (less than 0.03 wavefunction coefficients). This seems to exclude the possiblity that the antiferromagnetic interaction between the vanadium(IV) centers occurs by spin transfer through the phosphate bridges, as proposed for $VO(HPO_4)\cdot2H_2O$.[24] The results of the EH calculations for the V–P–O layer fragment $[V_8P_8O_{40}]^{4-}$ (with $V^{IV}/V^V = 1/1$) support qualitatively the proposed ferromagnetic and antiferromagnetic interactions of the unpaired electron at V^{IV} in the V–P–O layer consisting of the retracted-chair $V(OPO)_2V$ rings (Fig. 4).

References

1 Part 1, T. Yamase and K. Ohtaka, *J. Chem. Soc., Dalton Trans.*, 1994, 2599.
2 Part 2, T. Yamase, K. Ohtaka and M. Suzuki, *J. Chem. Soc., Dalton Trans.*, 1996, 283.
3 Part 3, T. Yamase, M. Suzuki and K. Ohtaka, *J. Chem. Soc., Dalton Trans.*, 1997, 2463.
4 A. J. Jacobson and J. W. Johnson, *Angew. Chem., Int. Ed. Engl.*, 1983, **22**, 412.
5 A. J. Jacobson, J. W. Johnson, J. F. Brody, J. C. Scanlon and J. T. Lewandowski, *Inorg. Chem.*, 1985, **24**, 1782.
6 M. R. Antonio, R. L. Barbour and P. R. Blum, *Inorg. Chem.*, 1987, **26**, 1235.
7 D. Papoutsakis, J. E. Jackson and D. G. Nocera, *Inorg. Chem.*, 1996, **35**, 800.
8 D. Beltrán-Porter, A. Amorós, R. Ibanez, A. LeBail, G. Ferey and G. Villeneuve, *Solid State Ionics*, 1989, **32**, 57.
9 D. Beltrán-Porter, A. Beltrán-Porter, P. Amorós, R. Ibanez, E. Martinez, A. LeBail, G. Ferey and G. Villeneuve, *Eur. J. Solid State Inorg. Chem.*, 1991, **28**, 131.
10 S. L. Wang, H. Y. Kang, C. Y. Cheng and K. H. Lii, *Inorg. Chem.*, 1991, **30**, 3496. Crystallographic data of **2** as follows: triclinic, space group $P\bar{1}$, $a = 6.2851(7)$, $b = 6.284(1)$, $c = 13.262(2)$ Å, $\alpha = 80.30(1)$, $\beta = 87.434(9)$, $\gamma = 89.94(1)°$, $V = 515.7(1)$ Å^3, $Z = 4$, $R = 0.0351$, $R_w = 0.0480$, for 2413 unique reflections.
11 K. H. Lii, N. S. Wen, C. C. Su and B. R. Chueh, *Inorg. Chem.*, 1992, **31**, 439; H. Y. Kang, W. C. Lee, S. L. Wang and K. H. Lii, *ibid.*, 1992, **31**, 4743.
12 P. Ayyappan, A. Ramanan and C. C. Torardi, *Inorg. Chem.*, 1998, **37**, 3628.
13 R. Sisková, L. Benes, V. Zima, M. Vlcek, J. Votinsky and J. Kalousova, *Polyhedron*, 1993, **12**, 181.
14 C. J. O'Conner, *Prog. Inorg. Chem.*, 1982, **29**, 203.
15 G. M. Sheldrick, *Crystallographic Computing 3*, eds. G. M. Sheldrick, C. Kruger and R. Goddart, Oxford University Press, 1985, p. 175.
16 N. Walker and D. Stuart, *Acta Crystallogr., Sect. A*, 1983, **158**, 3.
17 TEXSAN, Single-crystal Structure Analysis Software, Molecular Structure Corporation, The Woodlands, TX, 1989.
18 I. D. Brown and K. K. Wu, *Acta Crystallogr., Sect. B*, 1976, **32**, 1957.
19 D. Altermatt and I. D. Brown, *Acta Crystallogr., Sect. B*, 1985, **41**, 240; I. D. Brown and D. Altermatt, *Acta Crystallogr., Sect. B*, 1985, **41**, 144.
20 M. R. Bond, L. M. Mokry, T. Otieno, J. Thompson and C. J. Carrano, *Inorg. Chem.*, 1995, **34**, 1894.
21 G. S. Rushbrooke and P. J. Wood, *Mol. Phys.*, 1958, **1**, 257.
22 L. Lezama, G. Villeneuve, M. D. Marcos, J. L. Pizarro, P. Hagenmuller and T. Rojo, *Solid State Commun.*, 1989, **70**, 899.
23 M. E. Leonowicz, J. W. Jonson, J. F. Brody, H. F. Shannon, Jr. and J. M. Newsam, *J. Solid State Chem.*, 1985, **56**, 370.
24 G. Villeneuve, K. S. Suh, P. Amorós, N. Casan-Pastor and D. Beltrán-Porter, *Chem. Mater.*, 1992, **4**, 108.

Paper a909452k